Carbon nanotube—Based cold cathodes: Field emission angular properties and temporal stability

S. Iacobucci, M. Fratini, A. Rizzo, Y. Zhang, M. T. Cole, W. I. Milne, S. Lagomarsino, A. Liscio, and G. Stefani

---

Articles you may be interested in

Effect of oxygen plasma on field emission characteristics of single-wall carbon nanotubes grown by plasma enhanced chemical vapour deposition system
J. Appl. Phys. **115**, 084308 (2014); 10.1063/1.4866995

Effects of carbon nanotube diameters of the screen printed cathode on the field emission characteristics
J. Vac. Sci. Technol. B **28**, C2C41 (2010); 10.1116/1.3289316

Carbon nanotube tip melting with vacuum breakdown in cold cathode
J. Vac. Sci. Technol. B **25**, 1584 (2007); 10.1116/1.2770744

Direct growth of single-walled carbon nanotubes on conducting ZnO films and its field emission properties
Appl. Phys. Lett. **89**, 113116 (2006); 10.1063/1.2349296

Memory emission of printed carbon nanotube cathodes
Appl. Phys. Lett. **88**, 203108 (2006); 10.1063/1.2204576

Carbon nanotube—Based cold cathodes: Field emission angular properties and temporal stability

S. Iacobucci,[1,2,a)] M. Fratini,[1,3] A. Rizzo,[1,b)] Y. Zhang,[4] M. T. Cole,[4] W. I. Milne,[4,5]
S. Lagomarsino,[3] A. Liscio,[6] and G. Stefani[1]

[1]*Dipartimento di Scienze, Università Roma Tre, via della Vasca Navale, 84, 00146 Roma, Italy*
[2]*CNR-Istituto di Struttura delle Materia, c/o Dipartimento di Scienze, Università Roma Tre, via della Vasca Navale, 84, 00146 Roma, Italy*
[3]*CNR-Institute of Nanotechnology, c/o Physics Department, "Sapienza" University, Piazzale Aldo Moro 5, 00185 Roma, Italy*
[4]*Electrical Engineering Division, Department of Engineering, University of Cambridge, 9 JJ Thomson Avenue, CB3 0FA Cambridge, United Kingdom*
[5]*Research Institute of Electronics, Shizuoka University, Hamamatsu, Japan*
[6]*CNR-ISOF via Gobetti 101, 40129 Bologna, Italy*

The field emission (FE) properties of carbon nanotube (CNT)-based cathodes have been investigated on nanostructured surfaces grown by plasma enhanced chemical vapor deposition. The FE angular properties and temporal stability of the emergent electron beam have been determined using a dedicated apparatus for cathodes of various architectures and geometries, characterized by scanning electron microscopy and I–V measurements. The angular electron beam divergence and time instability at the extraction stage, which are crucial parameters in order to obtain high brilliance of FE-based-cathode electron sources, have been measured for electrons emitted by several regular architectures of vertically aligned arrays and critically compared to conventional disordered cathodes. The measured divergences strongly depend on the grid mesh. For regular arrays of individual CNT, divergences from $2°$ to $5°$ have been obtained; in this specific case, measurements together with ray-tracing simulations suggest that the maximum emission angle is of the order of $\pm 30°$ about the tube main axis. Larger divergences have been measured for electron beams emitted from honeycomb-structured cathodes ($6°$) and significantly broader angle distributions ($10°$) from disordered CNT surfaces. Emission current instabilities of the order of 1% for temporal stability studies conducted across a medium time scale (hours) have been noted for all cathodes consisting of a high number (10^4 and larger) of aligned CNTs, with the degree of stability being largely independent of the architecture. *Published by AIP Publishing.* [http://dx.doi.org/10.1063/1.4965860]

I. INTRODUCTION

The basis of modern vacuum nano-electronics came to the fore some forty-years-ago, following the work of Spindt.[1] The application of metallic thin-films coupled to electron beam microlithography to produce large area field emission (FE) sources from Mo tips became ubiquitous.[2] Si and W have also been widely used to produce emitters and sub-micro-scale tips by anisotropic etching or deposition techniques in order to enhance emission.[3,4] Carbon nanotubes (CNTs) allow for similar functional enhancement due to their unique morphology. However, CNTs have a wide range of additional key advantages over metallic tips; principally, they have a very low turn on field (defined here as the applied field necessary to produce an emitted current of $1 \mu A/cm^2$), associated with their intrinsically high aspect ratio "whisker-like" shape, which provides an optimum geometrical field enhancement.[2,5] Nanotube field-emitting surfaces do not deteriorate in moderate vacuum (10^{-8} Torr); a

significant functional advantage over difficult to fabricate W and Mo tips, which require a vacuum of 10^{-10} Torr.[6]

The strong covalent backbone of CNTs endows them with a physical inertness towards sputtering, chemically inertness to contamination, and they can potentially carry high current densities, many orders of magnitude higher than even the best metallic conductors, with an impressive resistance towards electro-migration.[7] In addition, when driven to high currents, their resistivity decreases so that they do not tend to suffer from electric-field-induced sharpening; a common cause of temporal instabilities in metal tip field emitters.[3] Much effort has been expended on producing field emitters capable of high emission currents, high temporal stability, and high spatial uniformity.[8] CNT-based electron sources clearly have interesting properties, such as low voltage operation,[9] good stability,[10,11] long lifetime,[8] and high brightness,[12] making them well suited to a diverse range of electron emission applications.

Understanding the relation between the macroscopic emission properties with the structure of individual CNTs (low-level architecture) and their distribution on the cathode (high-level architecture) remains scientifically challenging and is important for technological applications.[13] The current-voltage characteristics are strongly influenced by

---

a)Author to whom correspondence should be addressed. Electronic mail: stefano.iacobucci@cnr.it
b)Present address: ALBA SYNCHROTRON LIGHT SOURCE, Ctra. BP 1413 km. 3, 3 08290 Cerdanyola delVallès, Barcelona, Spain.

120, 164305-1

various parameters such as the CNT dimensions, shape and chemical state of the emitting apex, whereas the overall source emitting behavior depends critically on the CNT density (number of tubes per unit area) and the emitting area. The CNT arrangement, in terms of distribution and orientation, is expected to allow the fabrication of electron sources with extremely high brightness. Nonetheless, in order to obtain micro-spots, the major problem to be solved is the capability of controlling both the spatial spread of the electrons within the beam, alongside any emission temporal instabilities. In particular, the performance in terms of spot size achievable using CNT-based cathode sources is determined by the divergence of the FE-beam, which in turns depends on the emission angle at the emitting apex.[14] This second issue limits the manufacture-ability of an electron source or an array of electron sources with exactly the desired properties in a reproducible manner.[15] Among the investigations on temporal stability CNT based electron sources, Ulmen highlighted the improved emission stability of multi-wall-CNT (MWCNT) films grown by the catalytic thermal chemical vapor deposition (CVD) as compared to MWCNT films grown by the plasma-enhanced CVD (PECVD) method, explaining the difference to be due to the different graphitic order;[16] while Bormashov modeled the work function (WF) variations of the emitting surfaces due to adsorption/desorption of molecular layers to study long term FE stability of disordered CNT's.[17]

Mechanical flexing, due to anisotropic torque induction associated with the catalyst material, of the CNT has been suggested as one possible problem. This of course is not a problem in the mechanically stiffer field emitter materials typically used in vacuum nano- and micro-electronics. Under the high-field conditions needed for electron field emission, CNTs may flex thereby augmenting the orientation or stimulating a tube to bend, in a reversible/irreversible mode depending on the field intensity applied on a medium time scale (typically of the order of 30 min).[18] In addition, the irreversible decrease in length of CNTs, although less important than the one occurring in the case of metallic tips, has been proposed as a lifetime degradation mechanism caused, for example, by local plasma in the tip region, which deleteriously etches the CNTs.[19]

In the present work, our contribution is twofold; we have investigated the angular properties of large area FE cathodes consisting of different CNT architectures—namely, dot-array (array of individually ordered CNTs), square-comb, honeycomb, and "spaghetti-like") by measuring the angular divergence of the electron beam; second, we have studied the morphology-dependent temporal instability of the field electron emission process.

II. METHODS

A. Sample preparation

All arrays were fabricated using electron beam lithography on degenerately doped Si $\langle 001 \rangle$ over a typical area of $250 \times 250 \, \mu m^2$. Arrays formed from individual CNTs (dot-array cathodes) were DC magnetron sputtered with a 10 nm ITO diffusion barrier and 7 nm Ni catalyst, whilst the

hexagonal and square arrays were produced using a sputtered Al (10 nm)/F (1 nm) bilayer. Residual polymethyl-methacrylate resist was lifted off in acetone. In the case of the individual CNTs, synthesis was conducted by plasma-enhanced chemical vapor deposition in a commercially available Aixtron Black Magic system. CNT growth was stimulated by heating the catalyst samples to $700\,^{\circ}C$ ($5\,^{\circ}C/s$) at 5 mbar under 200 sccm NH_3:50 sccm C_2H_2 for 15 min. In the case of the hexagonal and square CNT arrays, thermal chemical vapor deposition was employed, at $520\,^{\circ}C$ ($5\,^{\circ}C/s$) at 25 mbar under an atmosphere of 192 sccm NH_3:8 sccm C_2H_2 for 5 min.

B. Electron beam ray tracing simulation

To optimize the extraction field and the emission angle, it is critical to control the angular properties of the FE and the geometry of the extractor. The angular properties of FE electron beams are strongly influenced by both the CNT architecture and the geometry of the extraction grid; all intimately impact the local field by modifying the average applied field due to the mutual screening between the emitting tips, which reduces the enhancement factor thus increasing the extraction threshold;[20] and the electrostatic field penetration through the apertures of the extraction grid (i.e., the grid mesh), which acts as a divergent lens on the electron trajectories (Calbick effect), resulting in an increase of the emitted electron beam pencil angle.[21]

In order to determine design guidelines for the experimental set-up, we first carried out simulations using a commercial ray tracing program.[22] The plane-capacitor fashion of the extracting diode typically used in the FE experiment was simulated as a flat mesh electrode (extracting grid) facing a flat continuous electrode (cathode) bearing the emitting tips. We modeled the CNTs as cylinders with the main axis coinciding with the applied electric field direction ($0°$ direction). These cylinders were surmounted by spherical shaped tips with radius of curvature $R = 25$ nm (this value coincides with the mean measured radius of curvature of the CNT tips of the dot-array cathode architecture used herein).[23] Each point of the tip acted as an individual source of randomly oriented electron trajectories emitted from $0°$ up to a maximum angle θ_{CNT}, with an initial kinetic energy of 200 meV.[24] We summed over the total number of trajectories (one thousand for each simulated configuration) and collected both the spatial and angular distributions of electron arrivals at the extracting electrode. A snapshot of the emission region from a single CNT is reported in the inset of Fig. 1(a), which displays trajectories starting from selected points, each one individuated by the angle θ included between the CNT axis **n** normal to the substrate and its position along the semi-sphere. The angle θ range is $(-90°, 90°)$. The corresponding initial condition for the (maximum) emission angle from CNT is defined by θ_{CNT}, whose range is $(\theta - 90°, \theta + 90°)$.

Due to the Calbick electrostatic lens effect, the mesh hole was found to be the most relevant parameter in the spread of the trajectories. Hence, in Fig. 1(a), the simulated electron beam divergence is plotted as a function of hole dimension while varying the CNT emission angle from $15°$
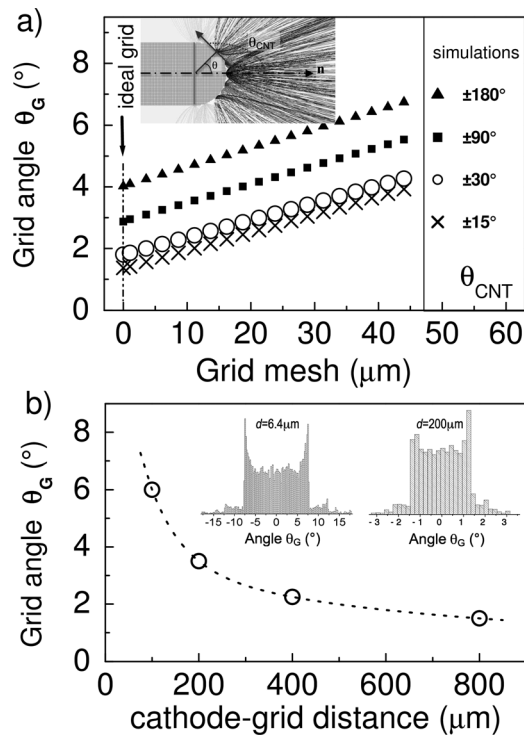
FIG. 1. Ray tracing simulations; (a) plot of the simulated e-beam divergence as a function of extracting grid mesh while varying the CNT emission angle from 15° to 180°; inset: a snapshot of the region around a single CNT emitting tip; (b) e-beam divergence as a function of cathode-grid distance considering CNT emission of ±90° around the tube axis and a grid with an aperture size (mesh) of 22 μm; inset: angle distribution of electron trajectories at different cathode-grid distances.

angle distributions collected on an ideal (continuous) grid located at $d = 6.4\ \mu$m at a potential $V = 70.6$ V and at $d = 200$ μm at $V = 2200$ V, respectively, hence upon a fixed applied field of 11 V/μm (it is worth noticing that, within the approximation of the simulation program, the effects of the local electric field already vanish at a few microns from the cathode). The explanation of the angle broadening for small d is the same as stated for lateral distributions in the paper of Siontas;[26] namely, that for decreasing cathode-grid distance d there is less available space for electron trajectories to be collimated by the electric field. Our simulations suggest that by increasing the cathode-grid distance the angular divergence decreases; however, when increasing this distance, to maintain the same extraction field, it is necessary to enhance the applied voltage, which implies that the grid must dissipate a significant and possibly problematic thermal load caused by impact of the accelerated electrons.

C. Experimental set up for field emission measurements

To measure the field emission angular properties, a specifically designed experimental apparatus was used. It is essentially a high vacuum chamber (base pressure 1×10^{-8} mbar) that hosts an extraction device and a Faraday-cup (FC). The latter is movable under vacuum by a three-axis manipulator and is equipped with a test ring of variable diameter that allows us to measure the angular distributions with different angular resolution. The extraction device (a picture is displayed in Fig. 2(a)) is made of two stainless steel plates; one holding the CNT cathode and the other
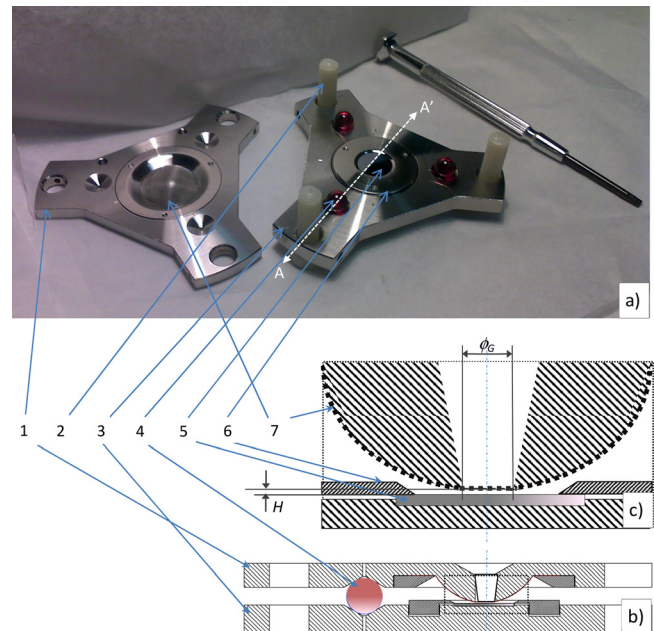
to 180°. Simulation results in Fig. 1 are obtained for an average electrostatic field of 10 V/μm, achieved by locating the extracting grid 200 μm from the cathode and parallel to its plane whilst applying a suitable potential of 2 kV. An increase in the applied field produced no significant variation of the angular distributions, and this value was fixed as a simulation benchmark, which was comparable with average fields typically applied in the experiment. For fixed θ_{CNT}, the divergence angle at the grid (θ_G) linearly increased with the mesh size and doubled when changing from a flat transparent extracting electrode ("ideal" grid) to a real-world, "thick" grid with a hole size of 50 μm. Notably, large hole sizes, though producing a significant increase in angle spread (from 4° to 7° for θ_{CNT} ranging from ±15° to ±90°), are nonetheless desirable for transmitting high current intensity.

To a lesser extent, the extractor-cathode distance also contributes to the beam divergence. In Fig. 1(b), the electron beam divergence is plotted as a function of the cathode-grid distance in the specific case of a grid with hole size of 22 μm, selected to obtain a good compromise between current transmission and angular spread, i.e., CNT emission at ±90° around the tube axis direction (such a conservative value is assumed to account for uncertainties of the correcting factors in the Fowler-Nordheim (FN) equations[25] and for irregularities expected in the shape of real CNTs). To highlight the effect of the cathode-grid distance d in contributing to the beam divergence, in Figure 1(b)-inset, we display the

FIG. 2. (a) Picture of the extractor during assembly; (b) section of the device along the AA′ direction; (c) magnification of the schematics showing the profile details of the emission region. Numeric labels indicate: (1) the extraction plate; (2) one of the mounting Teflon screws (removed after assembling); (3) the cathode plate; (4) one of the ruby spheres for electric insulation and mechanical alignment; (5) the cathode; (6) the cathode attachment ring; and (7) the extracting grid.

constituting the extractor element. They are separated by ruby spheres (diameter = 1.5 mm).

According to the simulation results, a compromise between the cathode-grid distance and the size of the grid holes is necessary to achieve the required extraction field whilst minimizing the electron beam divergence. The device geometry, displayed in the section drawing of Fig. 2(b), and its manufacturing have been optimized to obtain a suitable applied field (>10 V/μm) in order to achieve electron emission while overcoming the main dielectric insulation issues, namely, to avoid arcing and dielectric breakdown, and to minimize current losses. This has been achieved by polishing all metallic surfaces and by adopting a hemispherical profile (with a diameter of about 20 mm) for the extraction plate, so that the high field has been confined within a narrow region with a diameter $\phi_G = 2$ mm facing the cathode at a distance H of about 200 μm (Fig. 2(c)). The dielectric strength of the extraction device was determined by using an unpatterned Si chip: a loss current lower than 10 pA resulted for an applied field of 17.5 V/μm.

Simulations and previous experiments[27] evidenced the double role of the extraction grid: it contributes to the shape of the electron beam; in particular, it should produce a uniform field, while at the same time it should be sufficiently transparent to transmit a significant fraction of the electron beam; and finally, it should dissipate a substantial thermal load in the case of bright cathodes. For these reasons, several commercial grids of the type used in electron microscopy, with different mesh values (and hence effective transmission coefficients), have been mounted and tested. In all cases, they have shown severe limitations for both controlling beam divergence and thermal load issues. The best results for beam shaping have been obtained by using commercial copper mesh, suitably cut and pre-formed by a custom-made shaper device to fit the extractor hemispherical profile (see Fig. 2(c)). Nonetheless, to overcome the thermal load limitations (the measured thermal thresholds of the commercial grids did not reach 1 W), we have used two configurations to operate the extraction device: one configuration (integrated current mode) for high current intensity measurements, with the extractor element shut, allowing us to detect the total current emitted by the cathode; and another one (differential current mode) with the extractor element opened and equipped with a grid, allowing us to determine the transmitted current and the current distribution by measuring it in the FC, as described below.

Figure 3 shows a sketch of the electrical set-up used to measure the field-emission angular properties. The total current, I_{PW}, was measured using a picoammeter (Keithley model 485, A_1 in Fig. 3) inserted between the cathode plate and the power supply (Fluke model 410B). A second picoammeter (Keithley model 485, A_2 in Fig. 3) connected the grid to ground; a third one (Keithley model 6485, A_3 in Fig. 3) connected the FC to ground. The extracted current was measured up to a maximum value, compatible with the thermal load tolerable by the commercial grid (typically a few hundreds of mW). Note that the extraction field was produced by applying the accelerating voltage to the cathode plate and by grounding the extractor plate. This results in a field free region from the
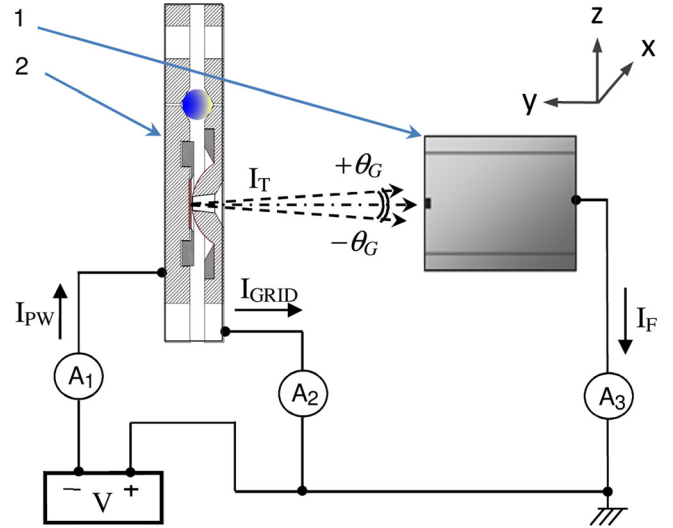

FIG. 3. Sketch of the electrical set-up for FE angular measurements: (1) movable Faraday cup and (2) schematics of the extraction device.

grid to the FC, and hence the angles of electron trajectories measured at the FC are the same as the angle at the grid, this being a non-trivial experimental advantage to measure current distributions by moving the FC.

The resulting transmission coefficient, T, is obtained using

$$T = I_T/(I_{PW}) \approx I_t/(I_{GRID} + I_T) \approx I_{FC}/\left(I_{GRID} + \int dx\,dz\,I_{FC}\right),$$

(1)

where I_T is the transmitted current. The total current I_{PW}, neglecting current losses, is given by the sum of the grid current (I_{GRID}) and I_T. For an ideally infinitesimal angular acceptance of the FC, I_T can be obtained by summing over the current intensity collected by the FC (I_{FC}) when moving in all positions within the xz-plane. I_T coincides with a single I_{FC} measurement within less than few percent, when the FC, located about 2 cm from the extractor, is equipped with an aperture 10 mm in diameter. In this case, we have measured $T \approx 0.27$ for a grid with a square mesh of 20 μm × 20 μm (bar × hole), in good agreement with the value of 0.25 expected from simple geometrical arguments.

Differential measurements of the emitted current have been performed by equipping the FC with a 0.5 mm diameter aperture, which allows for adequate resolution of the current distribution features. The beam axis coincides as a first approximation with the y-direction, as illustrated in Fig. 3. By scanning the FC in the two transverse directions (x, z) for fixed cup-cathode distance along the y axis, the spatial electron distribution has been measured. By repeating the measurements at different y values, the beam divergence angles (θ_G^x) and (θ_G^z) along the x and z directions, respectively, have been retrieved using

$$\theta_G^x = arctg\frac{\Delta x}{D}, \quad \theta_G^z = arctg\frac{\Delta z}{D},$$

(2)

where D is the distance between two different FC positions in the y direction; Δx and Δz are the difference of the full

width at half maxima (FWHM) of the spatial distributions along the x and z directions measured by the FC located at the two respective y positions.

D. Sample characterization

SEM images of several cathode architectures are shown in Fig. 4. In Section III, we compare the stability and angular properties of different cathodes assuming that the only variable affecting the emission is their different architecture, both at low- and high-levels. This is true as long as the surface electronic properties determining the tunnelling emission are the same. We tackled this issue by measuring the work function (WF) of all cathodes using the Kelvin Probe (KP) technique, which provides the contact potential difference (a.k.a. CPD) with a lateral resolution of 50 μm.

The direct quantification of the measured potential value was not trivial because of the contribution of the substrate due to the complex geometry of the samples strongly affected the measured potential values. Hence, KP measurements were first performed by sampling different cathode areas (typically $250 \times 250 \, \mu m^2$ for each sampled area) fixing the probe-sample distance at $\approx 50 \, \mu$m. The measured CPD values did not differ significantly, suggesting that the equipotential surface above the cathode is uniform. For this reason, taking into account that the probe-sample distance is larger than the height of the CNT array (typically 5 μm), we can roughly describe the probe-sample system such as a planar
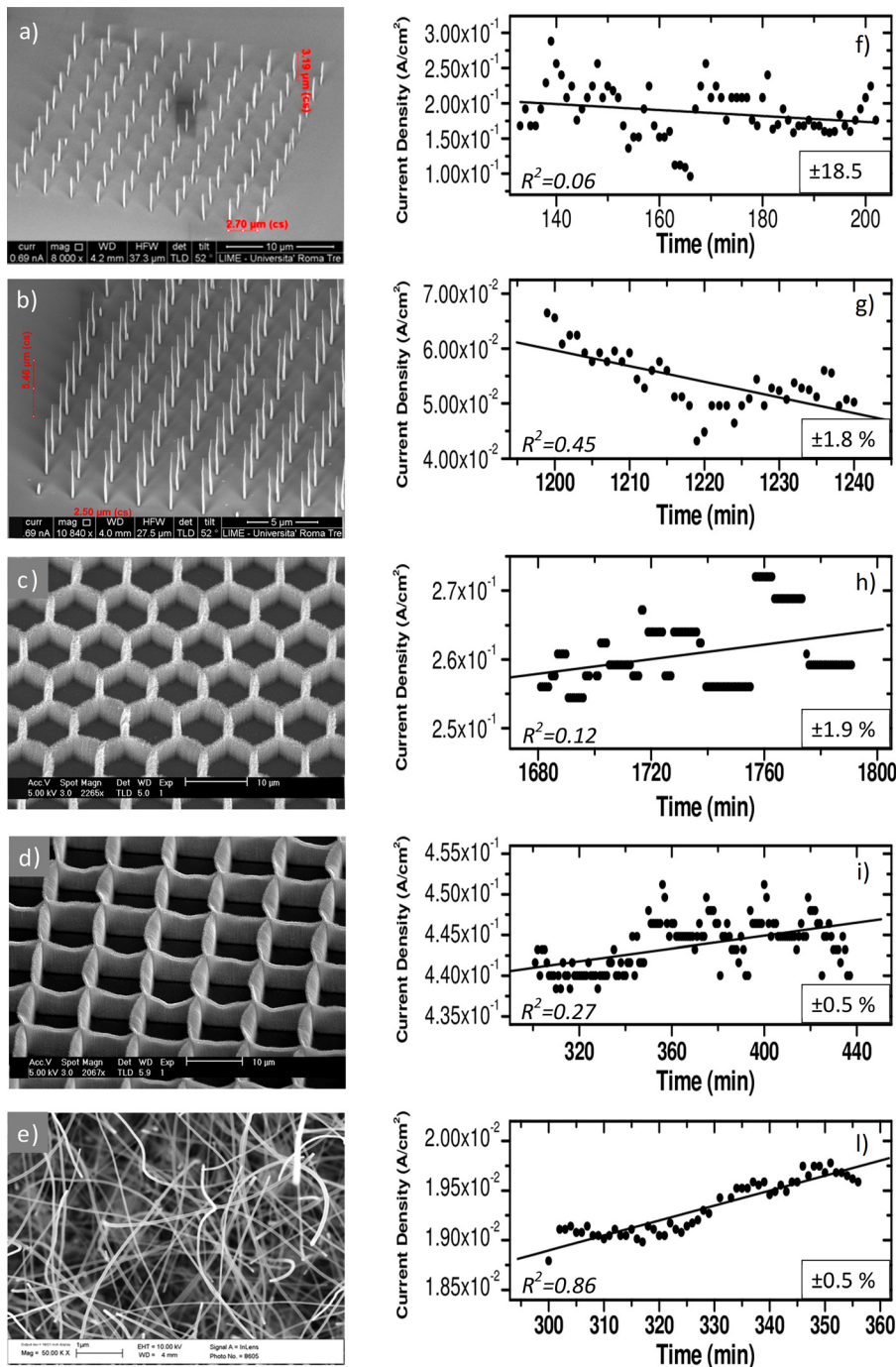

FIG. 4. Left: SEM images of the different CNT architectures. Right: medium time instability data (dots) with linear fits (line); on bottom of each panel, the R-square coefficients and the residual coefficients (percentage) are displayed on the left and right corner, respectively. Panels (a) and (f) refer to dot-array 100 tubes architecture cathode; (b) and (g) to dot-array 10^4 tubes; (c) and (h) to honeycomb; (d) and (i) to squared-comb; and (e) and (l) to disordered ("spaghetti-like") nano fibers.[31]

capacitor, within the experimental resolution, as in the case of the well-known macroscopic KP technique.[28] Repeating the same procedure for all the array architectures, we found that the achieved potential values varied in the range within 150 meV with respect to the graphite WF. Such differences would not dramatically shift the tunneling behavior. This evidence certainly supports the proposal that all the investigated materials have near equivalent band structure, at least as it pertains to the measured FE properties.

III. RESULTS AND DISCUSSION

A. Temporal stability

Temporal instabilities have been measured for several different CNT cathode architectures by monitoring both I_{PW} and I_{grid} as a function of time. In Fig. 4, typical behavior of I_{grid} densities vs time is reported (right panels) together with the respective SEM images (left panels). I_{grid} was measured after an activation procedure consisting of a first slow ramp-up of the extraction field (in steps of 10 eV/ 200 μm min) up to a maximum value of about 15 eV/μm, followed by a faster ramp-down (20 eV/200 μm min). The purpose of the activation procedure was to remove contaminants adsorbed during the cathode storage[17] and to reduce differences of CNTs length and orientation.[18] After this conditioning procedure, a reliable Fowler-Nordheim (FN) profile was noted for each sample, with each cathode then switched-on at a fixed operating voltage to produce an emitted current intensity ranging from few μA (for the individual 10^2 CNTs) to few hundred μA (for the spaghetti-like cathode). Fig. 4 shows a negative drift of a few percent, typically <20%, on a medium time scale (about 1 h), characteristic of the emission from the dot-array architectures, while a positive smaller drift (typically <2%) has been registered for the comb architectures and for the disordered cathode. A similar trend was found in the short time (<10 min) temporal instabilities for the various architectures. To quantify instabilities, a linear fit has been applied to raw data. The goodness of the fitting procedure can be statistically estimated by the R-square coefficients (R^2) that are displayed in the left-bottom corners in each case. The percentage values reported in Fig. 4 (right-bottom corners) correspond to the respective residuals of the short time fluctuations (dots) around the linear fits (line) of the experimental data. In particular, the individual 10^4 tube shows a much better stability (1.8%) with respect to the 10^2 tube one (18.5%), the ratio scaling statistically with the emitting tip (nominal) number. Taking into account the high density of emitting tips in the honeycomb architectures, their lower instabilities with respect to the 10^2 tube dot-array are in line with such statistically based observations, although a more quantitative comparison cannot be executed because, due to the electric field local distribution, only the peripheral regions of the CNT mesh in the honeycomb architectures are expected to contribute to the emission.[29] It is also worth noting that the medium time instability of the honeycomb structure in our work favorably compares with long time instability profile reported in.[29]

B. Electron beam angular profiles

Fig. 5 shows the divergence of the FE electron beam at the extracting grid for CNT cathodes with different architectures. The displayed values correspond to the FWHM of the angle distributions derived by the measured spatial distributions according to the procedure described previously. Data are reported as a function of the grid mesh upon fixing the other experimental conditions (applied extracting field = 10 V/μm, grid-cathode distance = 200 μm) according to the guidelines suggested by simulations. We have already shown that a maximum emission angle from the individual tips can be determined in the specific case of the dot-array. The linear fit ($R^2 = 0.5$) in Fig. 5 is for a dot-array cathode consisting of 10^4 CNFs, which is consistent with a maximum emission angle from the tips of $\pm 30^\circ$.[27] Interestingly, the intercept of the fitting does not coincide with the axis origin, which means that even in the case of an "ideal" grid a non-zero divergence is expected.

The complexity of the geometrical structure of the cathodes studied in the present paper prevents us from extending the same quantitative analysis to all architectures; nonetheless, to get information on the angular FE properties for all cathode samples, we focus our attention on the key physical parameters that contribute to the angle divergence across all samples. It is evident from Fig. 5 that ordered architectures produce more collimated electron beams with respect to disordered architectures. Considering the data subset obtained for a fixed grid mesh value of 20 μm, the evolution of the beam divergence with architecture complexity can be followed. The narrowest angle distributions are measured from well-ordered dot-array cathodes, which produce angles between 2° and 5°, a factor of two smaller than the ones obtained from hexagonal and square comb cathodes. Comb architectures are characterized by long-range order (regular structures few tens of microns wide), though at short-range (sub-micron level), their structure is much less regular than the dot-arrays. In this respect, comb architectures can be considered an intermediate step between individually ordered
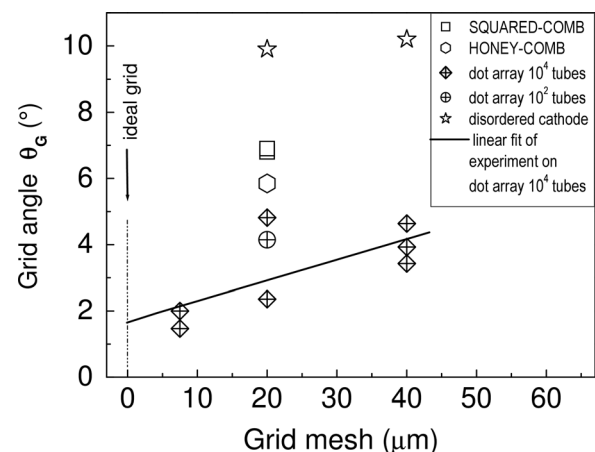

FIG. 5. Divergence of the FE e-beam measured at the extracting grid for CNT cathodes having different architectures. The continuous line is a linear fit of data from dot-arrays consisting of 10^4 tips and is consistent with maximum emission angle from the tips of $\pm 30^\circ$ around the normal direction to the cathode substrate, as derived from simulation results.[27]

emitting tips and the fully disordered emitting cathodes, like the "spaghetti-like." This last architecture produced electron beams that provide a factor of five more spread than the ones obtained from dot-arrays. Previous considerations synthetically assess that, broadly, to achieve low divergence electron beams, regular architectures are preferred with respect to disordered structures. Yet, to put things on a more quantitative perspective requires further analysis.

Both low-level architecture characteristics (namely, CNT individual structure) and high-level architecture ones (orientation distribution, density and uniformity of emitting tips) determine the FE properties;[13] in particular, both are expected to contribute to the angle divergence of the emitted beam. To obtain high brightness electron beams requires a high field enhancement factor (FEF) in FE from large area cathodes.[25,30] Uniformity in the CNT morphology better than 10%, over the entire emitter array in our CNT cathodes, as evidenced by SEM microscopy, is one of the necessary characteristics in order to obtain a high FEF. In this respect, the most efficient FE sources over the entire cathode area are the structures with the smallest surface curvature. To look for a dependence of the electron beam divergence on geometrical parameters at a low-level architecture, a reasonable attempt can be made by considering the thickness t and the height h of the individual emitting structure in each architecture and their ratio $R = t/h$, which is the inverse of the enhancement factor. R is defined in the dot-array case by taking for t the diameter of the CNT apex (50 nm) and for h the corresponding height of each individual nanotube (3 μm). In the case of honeycomb and square comb, we take for t the thickness (1 μm, 2 μm, respectively) and for h the corresponding height (8 μm, 12 μm, respectively) of the CNT superstructure constituting the array. We determined the corresponding parameters for the "spaghetti-like" cathode by an accurate inspection of the SEM images: it reveals the presence of several corners, namely, points of the long tubular structures where the nano-fibers are bent with a small curvature radius. It is conceivable that they are the nano-structures emitting with the highest efficiency over all the cathode area. The inspection allows us to set an average value of $t \approx h \approx 0.07$ μm. The result of such analysis is reported in Fig. 6(a), displaying the dependence of the experimental values θ_G vs R, from which significant considerations can be gathered: (i) the monotonic increase of θ_G with R is evident; (ii) for $R = 0$ a minimum value of $\theta_G \approx 3°$ is achieved. This value is attributed to the specific experimental conditions used (grid hole = 20 μm, cathode-extractor distance = 200 μm), which is in line with our simulations. The not-vanishing intercept has a generalized meaning: because of the presence of the extraction grid having a finite mesh size, even an ideal emitting structure with an infinitesimal radius of curvature will produce a not vanishing divergence of the electron beam, which we believe to be a significant result as it pertains to the design of high brilliance electron sources.

As discussed earlier, high-level architecture variations in our cathodes cannot be trivially quantifiable: their effect in determining the beam spread cannot be disentangled from the one given by low-level architecture variation (change of
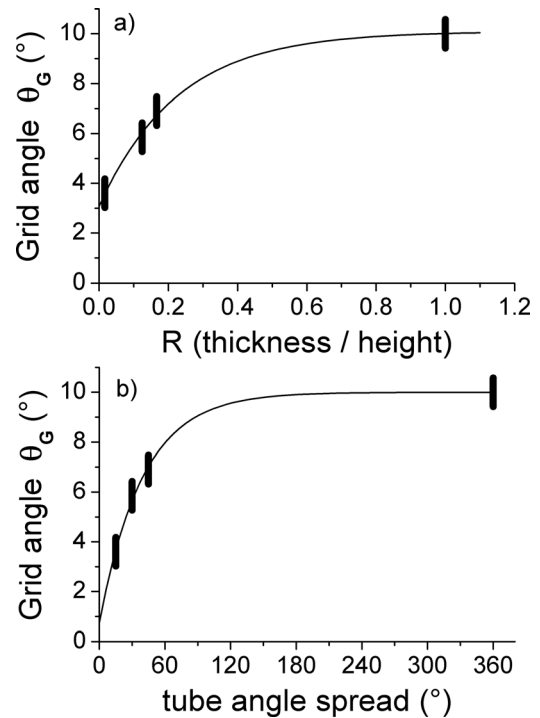

FIG. 6. Angular divergence at the extracting grid of the field emitted electron beam as a function of the CNT thickness over height ratio (panel (a)) and of the tube angular spread around the normal direction to the substrate (panel (b)), corresponding to different architecture cathodes. The continuous lines are guides for eyes. All measurements (rectangular dots) are performed with a grid mesh of 20 μm and for a cathode-extractor distance of 200 μm.

the ratio R). One of the parameters characterizing the high-level architecture is the orientation distribution of the tube axis.[13] Such distributions can be estimated from the SEM images and the angle spread of the tube orientation with respect to the normal to the substrate can be picked up for each architecture. In Fig. 6(b), the experimental values θ_G are plotted as a function of the angle-spread of carbon nanotubes: without assigning a specific meaning to the displayed profile, a straightforward information is nevertheless provided on the link between order/disorder and e-beam divergence.

IV. CONCLUSIONS

Here, we have rationalized the temporal stability and angular electron beam field emission properties of carbon-nanotube cathodes with different architectures, where we have correlated the time (in)stability and angular divergence with the corresponding structure. Our results show that cathodes with ordered architectures produce increasingly collimated electron beams with respect to disordered nanostructured cathodes, while time instabilities are correspondingly reduced when migrating from highly regular dot-arrays to square-comb and honey comb arrays, up to entirely disordered spaghetti-like structures.

ACKNOWLEDGMENTS

[1] C. A. Spindt, I. Brodie, L. Humphrey, and E. R. Westerberg, J. Appl. Phys. **47**, 5248 (1976).

[2] T. Utsumi, "Vacuum microelectronics—What is new and exciting—Keynote address," IEEE Trans. Electron Devices **38**, 2276–2283 (1991).

[3] W. Milne, S. Iacobucci, M. Fratini, Y. Zhang, L. Wei, C. Li, and M. T. Cole, in 19th International Display Workshops (IDW/AD'12) (Kyoto, Japan, 2012).

[4] C. Prommesberger et al., "Comparison of integral and local field-emission properties of Mo-coated p-Si tip arrays," in 28th International Vacuum Nanoelectronics Conference (IVNC), IEEE, 2015.

[5] C. J. Edgcombe and U. Valdrè, Solid-State Electron. **45**, 857 (2001); G. C. Kokkorakis, A. Modinos, and J. P. Xanthakis, J. Appl. Phys. **91**, 4580 (2002).

[6] R. H. Baughman, A. A. Zakhidov, and W. A. de Heer, Science **297**, 787 (2002).

[7] B. Q. Wei, R. Vajtai, and P. M. Ajayan, Appl. Phys. Lett. **79**, 1172 (2001).

[8] S. F. Ahmed, S. Das, M. K. Mitra, and K. K. Chattopadhyay, Indian J. Pure Appl. Phys. **44**, 700 (2006).

[9] N. S. Lee, D. S. Chung, I. T. Han, J. H. Kang, Y. S. Choi, H. Y. Kim, S. H. Park, Y. W. Jin, W. K. Yi, M. J. Yun, J. E. Jung, C. J. Lee, J. H. You, S. H. Jo, C. G. Lee, and J. M. Kim, Diamond Relat. Mater. **10**, 265 (2001).

[10] Y. Saito and S. Uemura, Carbon **38**, 169 (2000).

[11] F. Giubileo, A. Di Bartolomeo, M. Sarno, C. Altavilla, S. Santandrea, P. Ciambelli, and A. M. Cucolo, Carbon **50**, 163 (2012).

[12] N. de Jonge, Y. Lamy, K. Schoots, and T. H. Oosterkamp, Nature **420**, 393 (2002); N. de Jonge, J. Appl. Phys. **95**, 673 (2004).

[13] Y. Cheng and O. Zhou, C. R. Phys. **4**, 1021 (2003).

[14] M. Fratini et al., "Carbon-nanotubes field emitter to be used in advanced X-ray source," in Short Wavelength Laboratory Sources (Royal Society of Chemistry, 2014), p. 358.

[15] N. de Jonge and J.-M. Bonard, Philos. Trans. R. Soc., A **362**, 2239 (2004).

[16] B. Ulmen, V. K. Kayastha, A. DeConinck, J. Wang, and Y. K. Yap, Diamond Relat. Mater. **15**, 212 (2006); V. K. Kayastha, B. Ulmen, and Y. K. Yap, Nanotechnology **18**, 035206 (2007).

[17] V. S. Bormashov et al., Surf. Interface Anal. **39**, 155 (2007).

[18] Y. Wei, C. Xie, K. A. Dean, and B. F. Coll, Appl. Phys. Lett. **79**, 4527 (2001).

[19] K. A. Dean and B. R. Chalamala, Appl. Phys. Lett. **75**, 3017 (1999).

[20] R. G. Forbes, J. Appl. Phys. **111**, 096102 (2012).

[21] B. Lencovâ, in Handbook of Charged Particle Optics, edited by J. Orloff (CRC Press, Boca Raton, 1997), p. 188.

[22] Simulation code "Simion 3D" V.7.0-Idaho National and Environmental Laboratory-95/0403 7.1.

[23] E. Minoux, O. Groening, K. B. K. Teo, S. H. Dalal, L. Gangloff, J.-P. Schnell, L. Hudanski, I. Y. Y. Bu, P. Vincent, P. Legagneux, G. A. J. Amaratunga, and W. I. Milne, Nano Lett. **5**, 2135 (2005).

[24] N. de Jonge and N. J. Van Druten, Ultramicroscopy **95**, 85 (2003).

[25] J. Bonard et al., Phys. Rev. Lett. **89**, 197602 (2002).

[26] S. Siontas, A. Kyritsakis, J. P. Xanthakis, S. Iacobucci, and G. Stefani, J. Vac. Sci. Technol., B **32**, 02B107 (2014).

[27] S. Iacobucci, M. Fratini, A. Rizzo, F. Scarinci, Y. Zhang, M. Mann, C. Li, W. I. Milne, M. M. El Gomati, S. Lagomarsino, and G. Stefani, Appl. Phys. Lett. **100**, 053116 (2012).

[28] I. D. Baikie, S. Mackenzie, P. J. Z. Estrup, and J. A. Meyer, Rev. Sci. Instrum. **62**, 1326 (1991).

[29] C. Li, Y. Zhang, M. Mann, D. Hasko, W. Lei, B. Wang, D. Chu, D. Pribat, G. A. J. Amaratunga, and W. I. Milne, Appl. Phys. Lett. **97**, 113107 (2010).

[30] G. C. Kokkorakis and J. P. Xanthakis, Surf. Interface Anal. **39**, 135 (2007).

[31] S. Carta, "The 'spaghetti-like' cathode," private communication (2011).